

Multilevel NLTE radiative transfer in isolated atmospheric structures: implementation of the MALI-technique

P. Heinzel

Astronomical Institute, Academy of Sciences of the Czech Republic, CZ-25165 Ondřejov, Czech Republic

Received 7 September 1994 / Accepted 15 December 1994

Abstract. We have developed and extensively tested a new multilevel NLTE transfer code for isolated solar atmospheric structures (loops, prominences, spicules etc.). The code is based on the MALI approach of Rybicki & Hummer (1991, 1992) to multilevel accelerated lambda iterations. It is demonstrated that this method is fully capable of treating a difficult problem of NLTE hydrogen excitation and ionization equilibrium, provided that we *linearize* the preconditioned statistical equilibrium equations with respect to atomic level populations and the electron density. With this generalization of the original MALI approach, the numerical code is robust and stable. As compared to the standard linearization method of Auer & Mihalas (1969), the new MALI code designed for 1D slabs is *more than one order of magnitude faster* and its accuracy is quite satisfactory. We discuss several details of our implementation of the MALI technique to isolated, externally irradiated, 1D structures and finally draw some future prospects.

Key words: NLTE radiative transfer – methods: numerical – Sun: prominences

1. Introduction

Spectral diagnostics of isolated structures in the solar atmosphere becomes more and more important for several reasons. First, such structures like prominences, loops, spicules etc. represent the objects in the solar atmosphere which are now the subject of intense studies of many researchers (see papers in Ruždjak & Tandberg-Hanssen 1990 and Rušin et al. 1994). Second, some of these finite structures can be regarded as basic constituents of solar and stellar atmospheres (e.g. spicules, fibrils, quiet-atmosphere loops) and thus the detailed understanding of their physical behaviour plays a crucial role in the modelling of *inhomogeneous* atmospheres as whole (Fontenla et al. 1988; Heinzel 1991; Heinzel & Schmieder 1994). Finally, let us also mention that new large instruments are almost ready to start observations (SOHO, THEMIS) and they will provide us with a

Send offprint requests to: P. Heinzel

great wealth of high-quality spectroscopic data. Therefore, new efficient tools for spectral diagnostics and NLTE modelling are highly desirable.

In the present paper we test numerically the *multilevel* Accelerated Lambda Iteration (ALI) technique for the case of such isolated structures and demonstrate its ability and usefulness for practical use. For quiescent solar prominences (no velocity fields), a two-level ALI was already successfully applied by Paletou et al. (1993) and Auer & Paletou (1994). These authors undertook the difficult task to implement ALI to structures having 2D-slab geometry and they also accounted for the partial frequency redistribution (PRD) in resonance lines. For hydrogen $L\alpha$ line they confirmed its PRD-behaviour already studied for 1D slabs by Heinzel et al. (1987) and they recognized some new 2D effects. However, this work has been confined entirely to a schematic case of a two-level atom without continuum. On the other hand, Heinzel et al. (1987) (further referred to as HGV) and Gouttebroze et al. (1993) (referred to as GHV) have performed an extensive NLTE modelling of prominences and prominence-like structures, assuming 1D slab geometry, PRD and *multilevel* hydrogen atom model with continuum (up to 30 levels). Their results are important not only for resonance Lyman lines ($L\alpha$, $L\beta$, ...), but also for such important line as $H\alpha$ which is most frequently used line for prominence studies. Heinzel's code is based on the linearization method of Auer & Mihalas (1969) and uses an equivalent-two-level-atom (ETLA) approach to account for PRD (see Hubeny 1985 and HGV for ETLA formalism with PRD). A similar code developed by Gouttebroze uses only ETLA iterations together with PRD.

However, both these sophisticated codes are rather time-consuming, even when used on the Cray-2 machine. Therefore, it was highly desirable to test the possibility of applying fast ALI techniques for such huge multilevel computations in finite-size structures. Since there is strong interlocking between individual hydrogen atomic levels (including the continuum one) and the geometry (externally irradiated 1D slabs) is different from standard semi-infinite situations where ALI are now almost routinely applied - see papers in Kalkofen (1987) and Crivellari et al. (1991) - it was not evident a priori how a multilevel ALI

will work, i.e. the stability, convergence properties, accuracy, ionization equilibrium etc. To test this, we proceed here in the following way:

(i) We start with the *multilevel* ALI - so called MALI - approach recently proposed by Rybicki & Hummer (1991, 1992) (we shall refer to these papers as to RH1 and RH2) and apply it to a multilevel hydrogen atom with continuum. Our approximate lambda operator Λ^* is simply diagonal, as also suggested by these authors and by Auer & Paletou (1994) for the two-level case.

(ii) To obtain a MALI-based code for 1D prominence slabs, we just replaced the linearization part of our well-tested NLTE code by the routines relevant to MALI. This also enabled us to test the new results and properties of MALI code against those of the original linearization code - both codes have essentially the same structure and exactly same setup and inputs. For simplicity, we use in this paper only the complete redistribution (CRD) for Lyman lines, while MALI implementation with PRD will be reported in another paper.

2. Multilevel ALI technique applied to 1D slabs

Recent reviews of various ALI approaches and their numerical implementations to both solar and stellar semi-infinite atmospheres can be found in Crivellari et al. (1991), Hubeny (1992) and in the introduction to RH1. As it is now well established, the general idea behind all ALI methods is to split the exact lambda operator $\Lambda_{\mu\nu}$ (μ is the directional cosine and ν is the frequency) into two parts

$$\Lambda_{\mu\nu} = \Lambda_{\mu\nu}^* + (\Lambda_{\mu\nu} - \Lambda_{\mu\nu}^*), \quad (1)$$

where $\Lambda_{\mu\nu}^*$ represents so-called *approximate* lambda operator. Corresponding NLTE iteration procedure to obtain the depth-dependent intensity of the radiation field $I_{\mu\nu}$ is

$$I_{\mu\nu} = \Lambda_{\mu\nu}^* [S_{\mu\nu}] + (\Lambda_{\mu\nu} - \Lambda_{\mu\nu}^*) [S_{\mu\nu}^\dagger], \quad (2)$$

where $S_{\mu\nu}$ is the source function for a given transition (line or continuum), $S_{\mu\nu}^\dagger$ is its value from the previous iteration. If $\Lambda_{\mu\nu}^*$ is properly constructed (which is the art of all ALI methods), this accelerated lambda iteration will converge much faster than the ordinary lambda iterations. Several methods have been designed to implement this ALI procedure to various multilevel NLTE problems of stellar atmospheres and sophisticated codes now exist which are far superior to classical ones (i.e. standard linearization or ETLA).

In this paper we use the multilevel ALI technique to evaluate efficiently the excitation and ionization equilibrium of a hydrogen plasma in externally irradiated 1D slabs. We consider the same prominence models as in HGV and GHV, i.e. isothermal and isobaric plasma slabs, symmetrically irradiated on both sides by the incident diluted solar radiation. Note that a depth-dependent temperature and pressure structure was also recently considered (Rovira et al. 1994) and can be easily incorporated into the present formulation. We shall return to some details of

these prominence models in Sect. 4, but the reader can find all relevant information in the HGV and GHV papers.

Given the input parameters T , P , M and v_t (T - kinetic temperature, P - gas pressure, M - total column mass in direction perpendicular to the 1D slab, v_t - microturbulent velocity), the problem of constructing NLTE prominence models reduces to a solution of the radiative transfer equation for each explicitly treated transition (the radiation field for selected optically-thin transitions is held fixed and is given directly by diluted solar radiation), the set of stationary statistical equilibrium equations (ESE) and constraint equations like total particle-number and charge conservation. So in the following we shall concentrate mostly on this *restricted* NLTE problem. The difficulty arises due to unknown distribution of electron densities n_e inside the slab, i.e. the non-linear problem of hydrogen ionization equilibrium must be solved. The task would be much easier if we could consider n_e as given by the input model (instead of P for example) - in that case ESE are linear in the level populations. We discuss this question in Sect. 5.

As already mentioned in the introduction, our approach to this restricted NLTE problem closely follows the MALI ideas of RH1 and RH2 and the reader should consult these two papers for those details which are not explicitly described here.

2.1. Preconditioned ESE

Ordinary system of ESE for an atmospheric structure in a steady state has the standard form (Mihalas 1978, RH1, RH2)

$$n_i \sum_j (R_{ij} + C_{ij}) - \sum_j n_j (R_{ji} + C_{ji}) + n_i (R_{ik} + C_{ik}) - n_k (R_{ki} + C_{ki}) = 0, \quad (3)$$

where $i, j = 1, NL$ (NL being the number of atomic bound levels) and k denotes the continuum state. R_{ij} are bound-bound radiative rates, R_{ik} is the photoionization rate, while R_{ki} is the rate of radiative recombination. Using the notation of RH2, we can express the radiative rates generally as

$$R_{ll'} = \int d\Omega \int \frac{d\nu}{h\nu} (U_{ll'} + V_{ll'} I_{\mu\nu}), \quad (4)$$

where l and l' bring the values i, j for line transitions and i, k for the continuum ones. The auxiliary functions U and V have the classical form (Mihalas 1978, RH2)

$$\begin{aligned} U_{ij} &= \frac{h\nu}{4\pi} A_{ij} \phi_{ij}(\mu, \nu), \quad i > j \\ U_{ij} &= 0, \quad i < j \\ V_{ij} &= \frac{h\nu}{4\pi} B_{ij} \phi_{ij}(\mu, \nu) \end{aligned} \quad (5)$$

$$\begin{aligned} U_{ki} &= n_e \Phi_i(T) \frac{2h\nu^3}{c^2} e^{-h\nu/kT} \alpha_{ik}(\nu) \\ U_{ik} &= 0 \\ V_{ki} &= n_e \Phi_i(T) e^{-h\nu/kT} \alpha_{ik}(\nu) \\ V_{ik} &= \alpha_{ik}(\nu), \end{aligned} \quad (6)$$

where $\alpha_{ik}(\nu)$ is the photoionization cross-section and $\Phi_i(T)$ is the Boltzmann-Saha factor (see Mihalas 1978). A_{ij} and B_{ij} are the Einstein coefficients and $\phi(\mu, \nu)$ represents the normalized line profile function (in CRD approximation $\phi_{ij} \equiv \phi_{ji}$).

C_{ij} and C_{ji} are bound-bound collisional rates, C_{ik} and C_{ki} are the rates of collisional ionization and three-body recombination, respectively. If the electron density n_e , which appears in these rates, is known, then ESE are linear in the level populations including the continuum state (an additional relation must be added to get a closed system of $NL + 1$ linearly-independent equations - see next subsection for such constraints). The system of linear ESE can be easily solved for the level populations, provided that we know the radiation field in each transition which is critical for evaluating the radiative rates.

The basic idea of *preconditioning* is to eliminate analytically passive radiative terms in ESE, by means of approximate lambda operators Λ^* . This is fully described in RH1 and RH2. Preconditioning is thus used instead of linearizing the coupled system of transfer equations and ESE, which is strongly non-linear in the radiation fields and populations (so-called linearization method of Auer & Mihalas 1969). Preconditioning versus linearization is discussed in a review of Hubeny (1992). Various strategies of preconditioning ESE are developed in RH1 and RH2, where the general methods are described. However, any actual preconditioning strategy becomes problem-dependent and there is no need to use full preconditioning of RH2 in every case. In this paper we concentrate ourselves on the case of the multilevel atom with an active (resonance) continuum, but without any overlap between explicitly treated transitions. Such situation is very typical for hydrogen or some other species (CaII problem) in prominence-like structures.

In the case of hydrogen, the lines (first members of each series) can be treated either explicitly within the ALI-formalism, or for some of them the radiation intensity inside the structure is fixed by the diluted incident solar radiation (typically subordinate lines which are optically thin). These lines are non-overlapping. The only continuum treated explicitly is the resonance Lyman continuum (mostly optically thick - see GHV models), while other continua (subordinate) are optically very thin and thus their intensities are also fixed by the diluted incident solar radiation. These subordinate continua overlap among themselves and with the lines and we treat them as background continua in opacities. Their radiative rates in ESE are held fixed and are precomputed from diluted solar radiation.

In the following we shall formulate our preconditioning strategy which is basically identical to that described in RH1 (their Sect. 2.2), with simple generalization for the active continuum (which is anyway inherent in quite general formulas of RH2). The source function for a given frequency is written as

$$S_{\mu\nu} = r_x^\dagger S_x + (1 - r_x^\dagger) S_{bc}^\dagger, \quad (7)$$

where x is either ij for lines or c for continuum. The ratio r_x^\dagger takes the form

$$r_x^\dagger = \frac{\chi_x^\dagger(\mu, \nu)}{\chi_x^\dagger(\mu, \nu) + \chi_{bc}^\dagger(\nu)}, \quad (8)$$

where χ 's are the line, continuum and background (bc) opacities. As in RH1, all these quantities are taken from the previous iteration, which is again denoted by \dagger (otherwise the preconditioned ESE would not be linear in populations). The source function for background continua is S_{bc}^\dagger . In the present exploratory computations we neglect the electron scattering, which is anyway of low importance for most isolated structures.

The line source function takes the form

$$S_{ij}(\mu, \nu) = \frac{n_j U_{ji}}{n_i V_{ij} - n_j V_{ji}}, \quad (9)$$

which, assuming CRD, reduces to the standard formula for frequency-independent and isotropic line source function

$$S_{ij} = \frac{n_j A_{ji}}{n_i B_{ij} - n_j B_{ji}}. \quad (10)$$

The isotropic resonance continuum source function is written as

$$S_c(\nu) = \frac{n_k U_{k1}}{n_l V_{lk} - n_k V_{k1}}. \quad (11)$$

Using this formalism and Eq. (2), we can express the intensities of the radiation field as

$$I_{\mu\nu} = \Lambda_{\mu\nu}^* \cdot r_x^\dagger \cdot S_x + (\Lambda_{\mu\nu} [S_{\mu\nu}^\dagger] - \Lambda_{\mu\nu}^* \cdot r_x^\dagger \cdot S_x^\dagger) \quad (12)$$

$$J_\nu = \frac{1}{4\pi} \int I_{\mu\nu} d\Omega,$$

where x is again either ij (lines) or c (continuum) and J_ν is the mean intensity of the radiation field. Note that the terms with S_{bc}^\dagger have cancelled in this equation. Here we have replaced $\Lambda_{\mu\nu}^* [S_{\mu\nu}^\dagger]$ by ordinary product $\Lambda_{\mu\nu}^* \cdot S_{\mu\nu}^\dagger$, which is validated by the use of a diagonal Λ^* in this paper (Sect. 2.3).

According to RH1, we write for line transitions ij

$$\begin{aligned} \bar{J}_{ij} &= \frac{1}{4\pi} \int d\Omega \int d\nu \phi_{ij}(\mu, \nu) I_{\mu\nu} \\ &= \Lambda_{ij}^* \cdot S_{ij} + J_{ij}^{eff} \end{aligned} \quad (13)$$

$$\Lambda_{ij}^* \equiv \frac{1}{4\pi} \int d\Omega \int d\nu \phi_{ij}(\mu, \nu) \Lambda_{\mu\nu}^* r_{ij}^\dagger$$

$$J_{ij}^{eff} \equiv \bar{J}_{ij}^\dagger - \Lambda_{ij}^* \cdot S_{ij}^\dagger,$$

where \bar{J}_{ij} is the mean integrated intensity appearing in the bound-bound radiative rates and ϕ_{ij} is the line profile function. For the active continuum, J_ν is used instead of \bar{J} and we

can write

$$\begin{aligned} J_\nu &= \frac{1}{4\pi} \int I_{\mu\nu} d\Omega \\ &= \Lambda_c^*(\nu) \cdot S_c(\nu) + J_c^{eff}(\nu) \\ \Lambda_c^*(\nu) &\equiv \frac{1}{4\pi} \int \Lambda_{\mu\nu}^* r_c^\dagger d\Omega \\ J_c^{eff}(\nu) &\equiv J_\nu^\dagger - \Lambda_c^*(\nu) \cdot S_c^\dagger(\nu). \end{aligned} \quad (14)$$

The quantities J_{ij}^{eff} and J_c^{eff} are evaluated from the previous iteration.

Inserting these expressions into ESE, we obtain the preconditioned ESE which no longer contain the unknown radiation field intensities. The preconditioned ESE have essentially *the same form* as the ordinary ones, with the following replacements made

$$\begin{aligned} A_{ij} &\rightarrow A_{ij}(1 - \Lambda_{ij}^*) \quad (i > j) \\ \bar{J}_{ij} &\rightarrow J_{ij}^{eff} \end{aligned} \quad (15)$$

for line transitions, and

$$\begin{aligned} V_{1k} &\rightarrow V_{1k}[1 - \Lambda_c^*(\nu)] \quad (\text{photoionization}) \\ J_\nu &\rightarrow J_c^{eff}(\nu) \end{aligned} \quad (16)$$

for the active resonance continuum (integration over ν is then performed according to Eq. (4)).

These replacements represent a simple modification of ordinary ESE. Similar formalism can be used also for other species, if the explicitly treated transitions are non-overlapping. In the case of an overlap, a more sophisticated preconditioning strategy called *full preconditioning* (RH2) has to be used or one can linearize partially preconditioned ESE with respect to level populations.

2.2. Linearization of preconditioned ESE and constraint equations

For *given* electron density n_e , the set of preconditioned ESE is *linear* in atomic level populations, even when the active (Lyman in our case) continuum is included. However, if we want to solve ESE (together with the constraint equations) also for the unknown distribution of n_e , the problem becomes *non-linear* due to various products of n_e with the level populations including the continuum state. At low plasma densities, these terms are not critically important and thus an iterative solution of preconditioned ESE for atomic level populations is possible, keeping n_e and n_k ($n_e = n_k$ in our case) fixed during the solution of ESE. However, for medium and higher densities, non-linear terms start to play an important role and the convergence properties of such simple iterative procedure are not satisfactory. We have performed several numerical tests which indicate that even if a converged solution is apparently achieved, such a solution is not correct - the situation resembling a stabilization of the standard Λ iteration to a solution which is far from the true one.

To overcome these difficulties, we have *linearized* the preconditioned ESE with respect to all level populations, including

the continuum state n_k and the electron density n_e . We write the preconditioned ESE in a general form

$$F_i(n_j, n_k, n_e) = 0 \quad (i, j = 1, NL) \quad (17)$$

and the constraint equations (i.e. the total particle-number conservation and the charge conservation) as

$$\begin{aligned} (1 + \alpha) \sum_{j=1}^{NL} n_j + (1 + \alpha)n_k + n_e &= N \\ &= P/kT \\ n_k &= n_e \end{aligned} \quad (18)$$

(NL is the number of bound levels treated in ESE, N represents the total particle number density). α is the abundance ratio of He relative to H (helium is supposed to be neutral in the present exploratory computations, but we include it in order to obtain realistic plasma density ρ). Expansion of ESE and both constraint equations to the first order in the particle number densities leads to a set of linearized equations of the form

$$\begin{aligned} \sum_{j=1}^{NL} \left(\frac{\partial F_i}{\partial n_j} \right)_{n^\dagger} \delta n_j + \left(\frac{\partial F_i}{\partial n_k} \right)_{n^\dagger} \delta n_k + \left(\frac{\partial F_i}{\partial n_e} \right)_{n^\dagger} \delta n_e &= \\ -F_i(n_j^\dagger, n_k^\dagger, n_e^\dagger) \end{aligned} \quad (19)$$

$$\begin{aligned} (1 + \alpha) \sum_{j=1}^{NL} \delta n_j + (1 + \alpha)\delta n_k + \delta n_e &= \\ N - [(1 + \alpha) \sum_{j=1}^{NL} n_j^\dagger + (1 + \alpha)n_k^\dagger + n_e^\dagger] \\ \delta n_k - \delta n_e &= n_e^\dagger - n_k^\dagger. \end{aligned}$$

These equations are linear in δn_j , δn_k and δn_e and can be easily solved as a system of $NL + 2$ linear algebraic equations. Left-hand sides of first NL equations have the same structure as the ordinary ESE. n^\dagger denote the populations taken from the previous iteration. Once δn are evaluated, the new populations can be obtained as

$$n = n^\dagger + \delta n \quad (20)$$

(generalized Newton-Raphson iteration procedure). Complete iteration scheme is described in the next section. Note that in this approach we don't linearize ESE with respect to the intensities of the radiation field (as in complete linearization method of Auer & Mihalas 1969), because our linearized ESE have been preconditioned which already ensures a global coupling to the radiation field. As we shall demonstrate, this method works extremely well in the case of isolated atmospheric structures, as all our numerical tests do indicate.

2.3. Construction of diagonal Λ^* operator

Various forms of Λ^* have been used in the literature. This operator must satisfy two competitive conditions: (i) its form must

be as simple as possible to ensure the computational efficiency of the corresponding ALI method, and (ii) its form must reflect the basic features of the transfer problem, otherwise the satisfactory convergence is not achieved. Here we present two explicit forms of a diagonal Λ^* operator, which are used in our implementation of MALI. Note that our approach is different from that used for a two-level atom by Paletou et al. (1993) and Auer & Paletou (1994).

To construct the diagonal Λ^* operator, we proceed here in the following way. At any internal depth point d inside the slab we discretize the second-order transfer equation (Mihalas 1978)

$$-\frac{\mu^2}{\Delta\tau_-\Delta\tau}u_{d-1} + \left[1 + \frac{\mu^2}{\Delta\tau}\left(\frac{1}{\Delta\tau_-} + \frac{1}{\Delta\tau_+}\right)\right]u_d - \frac{\mu^2}{\Delta\tau\Delta\tau_+}u_{d+1} = S_d \quad (21)$$

$$\begin{aligned} \Delta\tau_- &= \tau_d - \tau_{d-1} \\ \Delta\tau_+ &= \tau_{d+1} - \tau_d \\ \Delta\tau &= (\Delta\tau_+ + \Delta\tau_-)/2 \\ d &= 2, \dots, D-1 \end{aligned}$$

($\mu \geq 0$ is the directional cosine, the frequency subscript ν was omitted). For static media, the standard Feautrier variable $u \equiv \frac{1}{2}(I_\mu + I_{-\mu})$.

Using the second-order boundary conditions (Auer 1967) for symmetrically irradiated 1D slab, we arrive at similar expressions at $d = 1$ and $d = D$ (D is the depth point at the center of the symmetrical slab)

$$\left(1 + \frac{2\mu}{\Delta\tau_+} + \frac{2\mu^2}{\Delta\tau_+^2}\right)u_1 - \frac{2\mu^2}{\Delta\tau_+^2}u_2 = S_1 + \frac{2\mu}{\Delta\tau_+}I^{inc} \quad (22)$$

$$\begin{aligned} \Delta\tau_+ &= \tau_2 - \tau_1 \equiv \Delta\tau_1 \\ d &= 1 \\ -\frac{2\mu^2}{\Delta\tau_-^2}u_{D-1} + \left(1 + \frac{2\mu^2}{\Delta\tau_-^2}\right)u_D &= S_D \end{aligned} \quad (23)$$

$$\begin{aligned} \Delta\tau_- &= \tau_D - \tau_{D-1} \equiv \Delta\tau_D \\ d &= D. \end{aligned}$$

$I^{inc} = I(-\mu, \nu)$ is the intensity of the incident solar radiation (see Sect. 3.3).

Now we can write, in a matrix form

$$\mathbf{T}\mathbf{u} = \tilde{\mathbf{S}}, \quad (24)$$

where \mathbf{T} is a tridiagonal matrix with the elements following from Eqs. (21) - (23), $\mathbf{u}=(u_1, \dots, u_D)$ and $\tilde{\mathbf{S}}=(S_1 + \frac{2\mu}{\Delta\tau_+}I^{inc}, S_2, \dots, S_D)$. Solving for \mathbf{u} we shall have

$$\mathbf{u} = \mathbf{T}^{-1}\tilde{\mathbf{S}} = \Lambda\tilde{\mathbf{S}}. \quad (25)$$

Full matrix Λ represents the exact Λ operator. According to Olson et al. (1986 - OAB), its diagonal is nearly optimum representation of Λ^* . However, an evaluation of Λ^* in this direct

way requires the inversion of the matrix \mathbf{T} and this is computationally prohibitive. Several approaches have been devised to effectively overcome this difficulty.

As suggested by OAB, one can approximately write

$$\begin{aligned} u_{d-1} &\simeq u_d e^{-\Delta\tau_-/\mu} \\ u_{d+1} &\simeq u_d e^{-\Delta\tau_+/\mu}. \end{aligned} \quad (26)$$

Inserting these expressions into Eqs. (21) - (23), we obtain the *diagonal* operator T^* , which is an approximation to the exact T . Then we can construct an approximate *diagonal* Λ^* operator as a simple inverse of the matrix elements

$$\Lambda_{dd}^* = (T_{dd}^*)^{-1} \quad (d = 1, \dots, D). \quad (27)$$

Final expressions for diagonal matrix elements of Λ^* take the form

$$\begin{aligned} \Lambda_{11}^* &= \left[\left(\frac{2\mu}{\Delta\tau_+} + 1\right) + \frac{2\mu^2}{\Delta\tau_+^2}(1 - e^{-\Delta\tau_+/\mu})\right]^{-1} \\ \Lambda_{dd}^* &= \left[1 + \mu^2\left(\frac{1 - e^{-\Delta\tau_+/\mu}}{\Delta\tau\Delta\tau_+} + \frac{1 - e^{-\Delta\tau_-/\mu}}{\Delta\tau\Delta\tau_-}\right)\right]^{-1} \\ \Lambda_{DD}^* &= \left[1 + \frac{2\mu^2}{\Delta\tau_-^2}(1 - e^{-\Delta\tau_-/\mu})\right]^{-1}. \end{aligned} \quad (28)$$

Another way of evaluating the diagonal elements of Λ^* operator was recently suggested by RH1. Their method is based on the original Feautrier scheme for solving Eqs. (21) - (23). Λ_{dd}^* are easily obtained during the formal solution of the transfer equation by the Feautrier method (in the backward sweep)

$$\Lambda_{dd}^* = (1 - D_d E_{d+1})^{-1} (B_d - A_d D_{d-1})^{-1}, \quad (29)$$

where

$$E_d = (B_d - C_d E_{d+1})^{-1} A_d \quad (E_{D+1} \equiv 0). \quad (30)$$

The coefficients A_d, B_d, C_d ($d = 1, D$) are those of the tridiagonal matrix \mathbf{T} and D_d corresponds to the standard Gaussian elimination scheme

$$D_d = (B_d - A_d D_{d-1})^{-1} C_d. \quad (31)$$

For details see the Appendix B in RH1.

Finally, for *static* structures, we can simply write (see Eqs. (13) and (14))

$$\begin{aligned} \Lambda_{ij}^* &= \int d\nu \phi_{ij}(\nu) r_{ij}^\dagger \int_0^1 d\mu \Lambda_{dd}^* \\ \Lambda_c^*(\nu) &= r_c^\dagger(\nu) \int_0^1 d\mu \Lambda_{dd}^* \end{aligned} \quad (32)$$

and these quantities enter the preconditioned ESE and their linearized equivalents through Eqs. (15) and (16). At $d = 1$, terms containing the expression $\Lambda_{11}^* \cdot (2\mu I^{inc} / \Delta\tau_1)$ will cancel in Eqs. (13) and (14) since they remain unchanged between the two consecutive iterations (similarly as in the case of background

continua). Therefore, the incident radiation affects the solution of our NLTE problem only through the term J_{ij}^{eff} or J_c^{eff} . In the formal solution of the transfer equation, an isotropic diluted incident radiation is used in the boundary conditions and the solution is performed consecutively for several selected μ). Finally, in order to get the emergent synthetic spectrum, we must distinguish between two different situations. First, the structure is observed on the solar limb (e.g. the prominences as treated by HGV and GHV) and then no incident radiation enters the slab *along the line-of-sight*. Second, the structures are seen in projection against the solar disk (like loops or mottles, see Heinzel et al. 1992 or Heinzel & Schmieder 1994) and then the *specific* intensity of the disk radiation along the line-of-sight enters the boundary condition when evaluating the synthetic spectrum.

All these equations can be easily generalized to a non-symmetrical 1D slab (i.e. irradiated only from one side, for example) or to other 1D geometries (symmetrical cylinders). We shall study these situations in other papers.

3. Numerical implementation of MALI

3.1. MALI code

In order to test numerically the implementation of MALI to 1D structures, we have modified our well-tested NLTE prominence code which is based on the standard linearization method of Auer & Mihalas (1969) (see HGV). We just replaced those subroutines in the linearization code which solve the non-linear system of radiative transfer and statistical equilibrium equations by new ones based on the MALI approach as described in the previous sections. In this way we obtained a new code which, however, has the same global structure and exactly same setup and input as the previous one. This allows us to compare, in a straightforward way, the results obtained with the MALI version (MALI code) against those obtained with the original linearization version (LIN code). The results obtained with the LIN code thus serve as benchmarks for our tests of the MALI code.

To be consistent with the LIN code, the formal solution of the transfer equation is performed using the standard Feautrier scheme (Mihalas 1978). Three angles are used to describe the anisotropy of the radiation field and 47 depth points cover one-half of the symmetrical 1D slab (we use the *log*-scale, with 5 points per decade). During each formal solution of the transfer equation, we evaluate simultaneously the approximate operators according to the formulas from Sect. 2.3. After extensive numerical experimentation we have realized that there exist various strategies how to proceed within one iteration cycle. In the computations discussed below we used the following scheme. First, opacities and emissivities are evaluated for current values of level populations. Then we perform the formal solution of the transfer equation which gives us the current radiation fields and approximate operators, for three angles. Then we solve the preconditioned ESE with current electron density - these equations are linear in atomic level populations. The updated populations finally enter the linearized set of preconditioned ESE, which are solved for corrections to level populations and electron density.

This procedure is repeated until the maximum relative changes in all populations and electron density (at all depths) are less than a prescribed value (typically 10^{-3}). After the convergence is reached, we evaluate the synthetic spectrum.

For tests we use a five-level hydrogen model atom with continuum. As in LIN, all optically-thick transitions are treated explicitly within the MALI formalism. These are all Lyman lines (in CRD), Lyman continuum, H α and H β (together 60 frequency points). The radiation field for the remaining transitions is held fixed and corresponds to the diluted incident solar radiation (see HGV and GHV for details). Incident radiation for explicit transitions is the same as in GHV (for the height $H = 10000$ km). Collisional rates are evaluated with the routine taken from Mihalas et al. (1975).

3.2. Initial hydrogen level populations

There are several useful strategies how to estimate the initial hydrogen level populations in prominence-like isolated structures. Populations of the lowest hydrogen levels are typically far from LTE values because, for lower gas pressures, the excitation and ionization of hydrogen is almost entirely driven by the incident solar radiation (see Table 1 in GHV for NLTE *b*-factors).

Once the *electron density* at the slab center had been somehow estimated, the initial hydrogen level populations can be determined as follows. Assuming a mixture of the hydrogen and helium atoms in a prominence plasma, we can write for the hydrogen ground-level population

$$n_1 \simeq [N - (2 + \alpha)n_e]/(1 + \alpha), \quad (33)$$

where $N = P/kT$ (total particle number density) and α is the abundance ratio of He relative to H (here $\alpha = 0.1$). $n_e = n_k$ (proton density) since the helium is supposed to be neutral. $n_1 \simeq n_{HI}$ (neutral hydrogen density), populations of excited hydrogen levels are several orders of magnitude lower than n_1 - see Table 2 in HGV paper. Then accordingly to several authors (e.g. Heinzel et al. 1994)

$$n_2 \simeq \text{const } n_e^2, \quad (34)$$

where the constant is of the order of 10^{-17} . Initial populations of higher levels are taken to be in LTE, for given temperature and electron density

$$n_i \simeq n_i^* = n_e^2 \Phi_i(T) \quad (i > 2). \quad (35)$$

For higher-pressure models it may be better to start with LTE even for n_2 , i.e. $n_2 \simeq n_e^2 \Phi_2(T)$. Moreover, if $n_1 < 0$ for given estimate of n_e , we either lower initial n_e in Eq. (33) (we recommend this) or evaluate all initial level populations in LTE for starting value of the electron density.

For an assumed prominence model, initial slab-center electron density can be estimated using the extensive tables of GHV or the relation between the gas pressure P and n_e (Heinzel et al. 1994). It follows from our experience with numerical implementation of the MALI technique to prominences that in some

cases the convergence is faster when starting with somewhat lower n_e than indicated above.

These estimates of initial n_e (also denoted as n_e^0) and n_i have been made for slab center and used at all other depths. In fact, approaching the slab surface, the convergence of our NLTE problem is not critically dependent on the initial populations, particularly for strongly irradiated, low-density isothermal structures.

3.3. Evaluation of I^{inc}

Assuming an isotropic incident radiation, $I^{inc} \equiv J_\nu^{inc} = 1/2 \int_{-1}^1 I_{\mu\nu}^\circ d\mu$. $I_{\mu\nu}^\circ$ is the limb-darkened incident solar radiation intensity. J_ν^{inc} is simply the mean intensity of the incident solar radiation field, at a given height above the solar surface. Note that our 1D formulation of the transfer problem requires that I^{inc} is symmetrical around the axis $\mu = 1$, i.e. the axis perpendicular to the slab. We use two possibilities how to evaluate J_ν^{inc} :

(i) We assume no center-to-limb variations (i.e. darkening or brightening) of I° , which leads to the relation $J_\nu^{inc} = I_\nu^\circ(\mu = 1) \times W$. $I_\nu^\circ(\mu = 1)$ is the solar radiation specific intensity as measured at the disk center and W is the classical dilution factor

$$W = \frac{1}{2} \left[1 - \left(1 - \frac{R^2}{(R+H)^2} \right)^{1/2} \right]. \quad (36)$$

R and H stand for the solar radius and the height of the structure above the solar surface, respectively.

(ii) Assuming the limb variations of the incident radiation, we get $J_\nu^{inc} = 1/2 \int_{-1}^1 I_{\mu\nu}^\circ d\mu$. This integral can be evaluated numerically, e.g. using the approach of Heinzel (1983).

To evaluate J_ν^{inc} for hydrogen transitions, we use the variant

(i) for all UV-transitions (i.e. the Lyman lines and continuum) and (ii) for all subordinate lines (Balmer, Paschen, etc.) - for details see HGV and GHV. Generally speaking, all NLTE models of isolated solar structures (prominences) are very sensitive to boundary conditions and to the incident radiation intensities involved in them.

4. Results of numerical tests with the MALI code

4.1. GHV-models used for tests

In order to test our MALI code, we use several representative models from an extensive GHV grid. However, we don't compare GHV results directly to ours, but rather we use these models together with the LIN code in order to obtain NLTE benchmark solutions. Computations have been performed for models with a typical prominence temperature $T = 8000$ K and for extremal gas pressures and geometrical thicknesses, according to GHV (see Table 1 for selected GHV models).

4.2. Convergence properties

All MALI computations have been performed using the linearization of preconditioned ESE. This leads to very favourable

Table 1. GHV models used for MALI tests

#	T K	P dyn cm ⁻²	M g cm ⁻²	D km	v_t km s ⁻¹	n_e^0 cm ⁻³
57	8000	0.01	5.676E-7	500	5	3.8E09
63	8000	1.00	7.786E-5	500	5	1.9E11
74	8000	0.10	2.759E-5	2000	5	2.7E10
78	8000	0.01	5.630E-6	5000	5	3.8E09
81	8000	0.10	6.791E-5	5000	5	2.8E10
84	8000	1.00	7.206E-4	5000	5	2.5E11

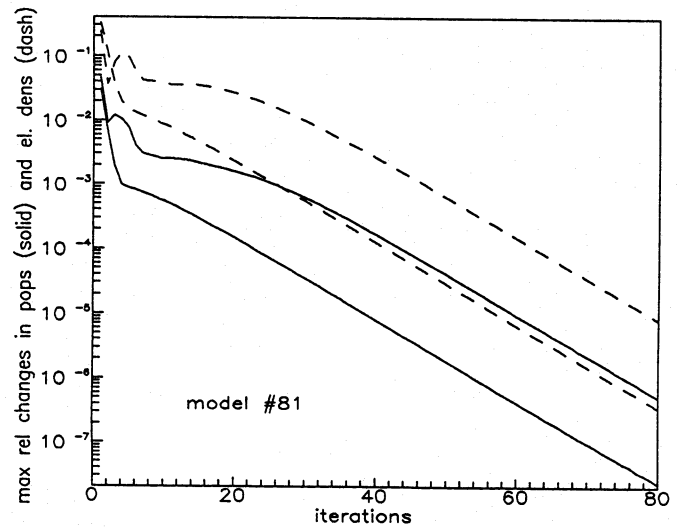


Fig. 1. Convergence plot for the model #81. 80 MALI iterations with linearized ESE are displayed. Upper pair of curves corresponds to initial LTE populations, lower one to a NLTE initial guess

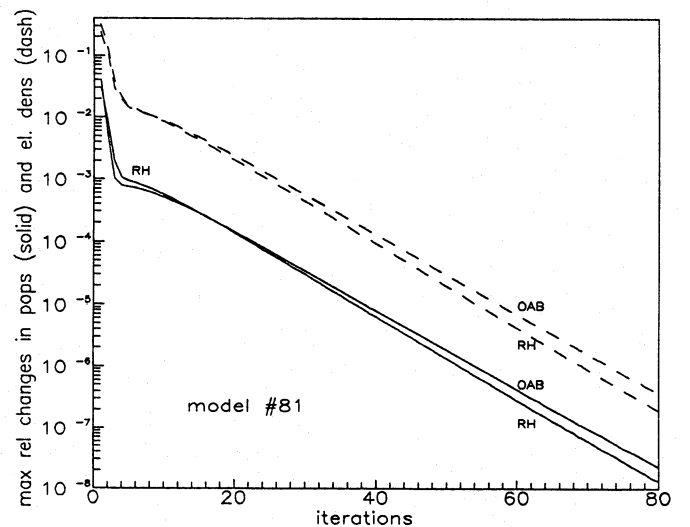


Fig. 2. Comparison of convergence properties of OAB and RH1 diagonal Λ^* operators. A NLTE initial guess of the level populations was used

convergence properties, even when no acceleration is used. The rate of the convergence typically depends on the atmospheric model and on the starting estimate of the electron density and hydrogen level populations. In Fig. 1 we show a typical example of the convergence properties pertinent to OAB-operator. Maximum relative changes (for all depths) in all hydrogen level populations and the electron density ($\Delta n_i/n_i$ and $\Delta n_e/n_e$) have been plotted for each iteration of MALI. We have started with a constant n_e^0 through the slab (Table 1). The convergence is much better if we start with NLTE level populations estimate suggested above. With LTE populations as an initial guess we see certain oscillations at the onset of the iterative procedure which results in a slower convergence. In Table 2 we summarize the results obtained for most typical prominence models with $T = 8000$ K. In the individual columns we give respectively the number of iterations necessary to achieve the *relative* accuracy 10^{-3} and 10^{-4} (i.e. the maximum value as can be inferred from figures like Fig. 1). We see that higher-pressure (or density) models typically require more iterations, both for MALI and LIN cases. In Fig. 2 we compare the convergence properties of OAB and RH1 diagonal operators, for a typical prominence model #81. We see very similar behaviour of both these operators, as also found by Hubeny (1994) in other situations.

From Table 2 we can estimate the relative speed of both codes. All computations have been performed on the Digital VAX-Station 3100 (under VMS-operating system) and a mean CPU-time per iteration was about 50 sec for LIN, 2 sec for MALI with OAB operator and around 1 sec for MALI with RH1 diagonal operator. With the numbers of iterations from Table 2 we may conclude that the present version of the MALI code is *more than one order of magnitude faster* as compared to the LIN code. A proper implementation of acceleration schemes (Ng or ORTHOMIN) should further improve the convergence rate. Note also that MALI code requires much less computer memory (LIN works with large matrices).

We have made several tests also for other GHV models with lowest (4300 K) and highest (15000 K) temperatures. The results are quite similar to those reported above. Moreover, for some low-temperature models we have met certain difficulties to reach the convergence with the LIN code, while MALI has been proved to be stable in all cases.

Finally, in Figs. 3 and 4 we demonstrate the convergence properties of MALI as compared to those of *standard lambda iterations* for model #81. The failure of standard lambda iterations in the case of a two-level-atom source function is well known (see e.g. Auer 1991). Here we demonstrate the *multi-level* behaviour by plotting the source function for $L\alpha$ and $H\alpha$ lines versus depth, for several iterations. Again, an unfavourable behaviour of lambda iterations is clearly evident, namely for optically thick ($\tau_0 \simeq 10^6$) $L\alpha$ line (100 iterations are plotted). The situation is less critical for $H\alpha$ which has $\tau_0 \simeq 1$, but non-linear multilevel coupling still causes important departures from the correct solution, particularly at the slab center. On the contrary, MALI converges within about 30 iterations to the same solution as obtained with the LIN code (at the beginning we have per-

Table 2. Convergence and accuracy

#	MALI (10^{-3})	LIN (10^{-3})	MALI (10^{-4})	LIN (10^{-4})	Δ %
57	7	4	37	5	0.9
63	31	12	48	15	3.2
78	13	5	27	7	0.8
81	26	10	42	14	2.0
84	38	15	56	22	3.1

formed 5 lambda iterations to smooth the initial guess). Depths in Figs. 3 and 4 are represented by the numbers of individual grid points. Since we use the *log-scale* for the depth grid, first 20-25 points correspond to the region where $H\alpha$ is almost completely transparent. Therefore, $S(H\alpha)$ can be regarded as practically constant in the 1D slab for lower-pressure models (see also GHV). An increase of the $H\alpha$ source function towards the slab surface takes place in the region of $L\beta$ line formation and thus seems to be related to multilevel interlocking effects.

4.3. Accuracy

The benchmarks computed with the LIN code allowed us to estimate an "absolute" accuracy of the MALI code. To do this, we have computed for each model from Table 1 (through all depths) the maximum relative difference for all level populations and n_e between MALI and LIN solution

$$\Delta \equiv \max \left| \frac{n_i(\text{MALI}) - n_i(\text{LIN})}{n_i(\text{LIN})} \right|. \quad (37)$$

We can see in Table 2 that Δ (in %) varies for typical models between 1 to 3 %. Although both LIN and MALI codes have basically same setup and we use the exactly same input data, this rather unimportant difference persists apparently due to quite different numerical approaches to solve the non-linear NLTE problem (linearization versus preconditioning). Similar conclusions have been made also by Hubeny (1994). Note also that heavy comparisons and tests between the LIN code and ETLA-based code of Gouttebroze (see GHV paper for discussion), using again exactly same input, led to Δ equal to a few %. RH1 have achieved an accuracy of about 1% for their MALI-L solution (ESE linear in level populations, n_e given), as compared to the benchmark ETLA solution of NLTE line transfer in a three-level hydrogen atom without continuum, performed by Avrett & Loeser (1987). We envisage that Δ could be lowered by using a finer depth grid.

5. Models parametrized by the electron density

5.1. General comments

In all previously discussed computations we have used as a basic model parameter set (T, P, M, v_t), i.e. isobaric-isothermal models. As the output we get consistently the depth-dependent

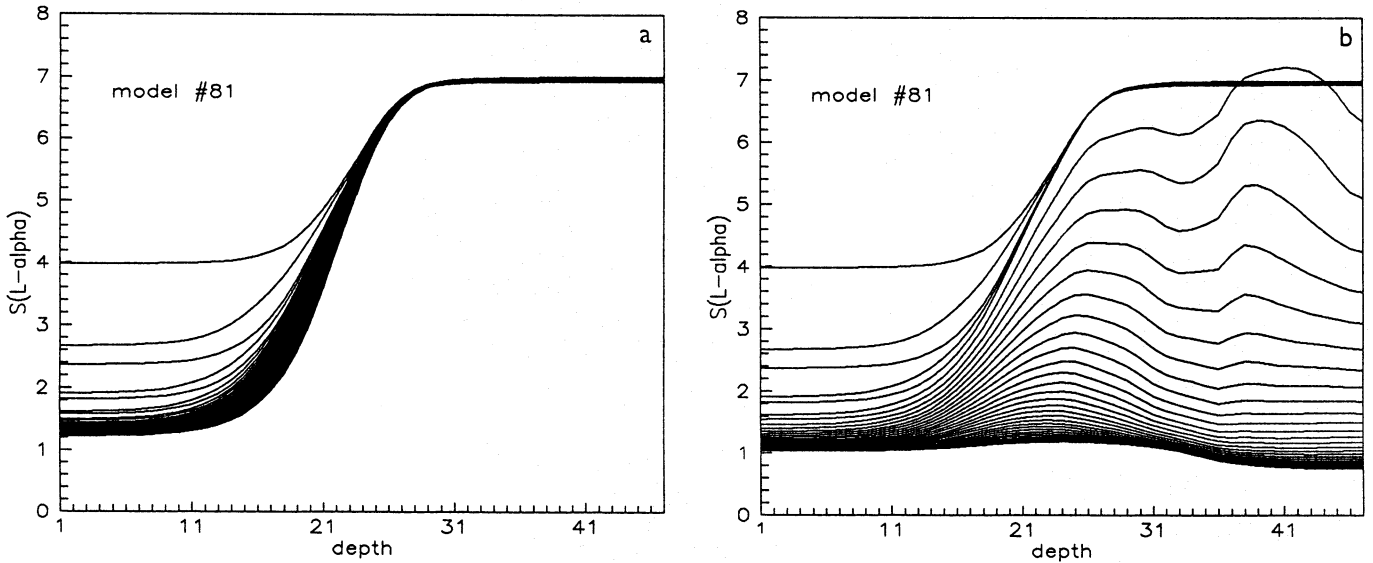


Fig. 3. **a** Convergence properties of ordinary lambda iterations. Depth variations of the $L\alpha$ line source function are shown for 100 iterations and for model #81. Depth points span the half of a symmetrical 1D slab, with $d=1$ at the surface and $d=47$ in the slab center. S is expressed in units of the line-center intensity. **b** Convergence properties of MALI iterations. Depth variations of the $L\alpha$ line source function are shown for 30 iterations and for model #81

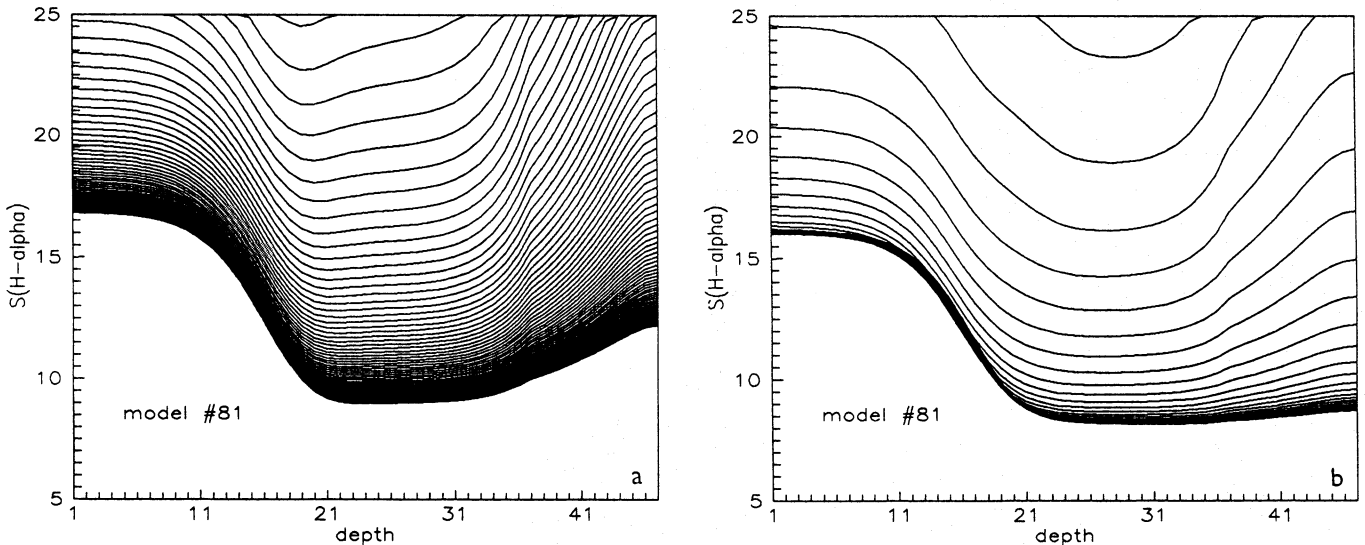


Fig. 4. Same as in Fig. 3. but for the $H\alpha$ line. Here S is expressed in % of the disk-center continuum near $H\alpha$

n_e and the gas density ρ , which gives the geometrical thickness $D = \int_0^M (1/\rho) dm$. This is a *fundamental* approach since T and P represent the basic thermodynamical plasma parameters which are coupled to other quantities through the MHD equations (a generalization to depth-varying T and P is straightforward). Ionization structure of the atmosphere is then consistently evaluated using the *linearized* preconditioned ESE.

However, in some cases we are directly interested in the electron density of the structure, which means that we want to specify the set (T, n_e, D, v_t) . n_e is then assumed to be constant through the slab, which is approximately true for most prominence-like, isobaric-isothermal models, as follows from

GHV tables. For the analysis of $H\alpha$ -line MSDP observations in terms of (T, n_e, D, v_t) see e.g. Wiik et al. (1992), Heinzel & Schieder (1994) or Schieder et al. (1994). In the case of prescribed n_e , one can use the *linear* set of preconditioned ESE to solve the NLTE problem, no linearization (Sect. 2.2) is necessary. After the convergence is achieved, we may finally evaluate P and ρ . However, this simpler MALI approach (linear ESE), although practical in some cases, is not fully equivalent to the fundamental one with the input $(T, P, M$ or $D, v_t)$. The reason is that depth-variations of P generally follow from MHD equations, while depth-variations of n_e come partly from depth-dependence of P and partly from NLTE ionization struc-

ture of the atmosphere. For example, in the case of a hydrostatic equilibrium, we can directly obtain the run of pressure with the column mass m , $P = mg$ (g is the gravitational acceleration, P is the total pressure), but we cannot prescribe physically realistic depth variations of n_e unless the non-linear NLTE problem is solved. For some quiescent prominence models, pressure balance leads to an isobaric structure for which n_e is however depth-dependent. Assuming n_e to be constant, we shall arrive at depth-dependent P which is unrealistic for these specific models.

5.2. Partial-redistribution effects

Considering further the models parametrized by the electron density, we have nevertheless found one very important advantage of such approach if applied to an analysis of $H\alpha$ observations. Namely, we can easily avoid rather complicated solutions with partial frequency redistributions (PRD) in resonance Lyman lines. As discussed by HGV, $H\alpha$ line intensity as well as n_e are affected by PRD through multilevel interlocking. For low-density models, the integrated $H\alpha$ intensity can be higher in PRD-case by about 30% as compared to CRD-case and also n_e in the slab center is higher. Therefore, a detailed analysis of high-quality $H\alpha$ data requires the full PRD approach (MALI modelling with PRD of Hubeny & Lites (1994) will be described in a subsequent paper). However, since $H\alpha$ itself is normally treated within CRD approximation (HGV, GHV, Hubeny & Lites 1994), we can use the present MALI/CRD code with the input set (T, n_e, D, v_t) to get *realistic* $H\alpha$ intensity as it would be evaluated with fully PRD code. The reason is that $H\alpha$ and other Balmer lines are strongly coupled to the electron density (Heinzel et al. 1994) and it is n_e which is primarily affected by PRD effects. Moreover, Lyman lines are optically very thick in the region of $H\alpha$ line formation (approaching the detailed radiative balance), so that it is of low importance whether we take CRD or PRD when evaluating their radiative rates.

To check this idea, we have made test computations for GHV model #74 (Table 1) for which detailed PRD solution with a 5-level atom plus continuum was obtained by using our LIN/PRD code (see HGV for description of this code). The slab-center n_e , evaluated by LIN/PRD code, was subsequently used as the input (i.e. n_e constant) in the version of MALI code with linear preconditioned ESE. The resulting integrated $H\alpha$ intensity is almost exactly same as that obtained by LIN/PRD code, with difference less than 1%. Also the populations of all *excited* levels agree quite well which we explain by strong coupling of these levels to the continuum state and thus to n_e ($n_e = n_k$ which is the same in both LIN/PRD and MALI computations). Of course, n_1 and the intensities of Lyman lines and Lyman continuum are inconsistent with PRD solution by a significant factor and the computed gas pressure is also different from PRD-value. For this model, a true difference between PRD and CRD $H\alpha$ integrated intensities (i.e. for given $P = 0.1 \text{ dyn cm}^{-2}$) amounts to 43%.

Therefore, we see that such an approach to $H\alpha$ line formation leads to very reasonable results, while inaccuracies caused by assuming a constant electron density can be of a secondary

importance. Moreover, putting the Lyman transitions into detailed radiative balance in ESE, we will substantially lower the number of frequency points in MALI solution. In this way we can obtain an extremely fast and relatively accurate *approximate* method of computing the Balmer lines intensities, particularly $H\alpha$. This can be easily coupled to velocity fields.

6. Conclusions

We have developed a new multilevel NLTE transfer code for 1D isolated atmospheric structures, based on the MALI approach of RH1 and RH2. In its present CRD-version, this MALI code was applied to a 5-level plus continuum hydrogen problem. It was extensively tested against the benchmark results provided by a similar code but based on the linearization method of Auer & Mihalas (1969) (LIN code of HGV). All tests have been performed with selected models of GHV.

It was demonstrated that the MALI approach is fully capable of treating the hydrogen excitation and ionization balance in such isolated, externally irradiated, 1D structures (slabs in this paper), provided that the preconditioned statistical equilibrium equations (ESE) are *linearized* with respect to all atomic level populations and the electron density. This linearization, which represents a generalization of the original MALI approach, is necessary for evaluating the hydrogen ionization structure inside the 1D slabs. The method works equally well for semi-infinite atmospheres. However, for certain class of models where a constant electron density is used as the input (i.e. n_e is known), the preconditioned ESE are linear in level populations. By comparing with the original LIN code of HGV, MALI code is *more than one order of magnitude faster* for typical model situations, depending on the choice of Λ^* operator. Also the accuracy of the MALI code was found to be quite satisfactory, as tested on GHV models. The MALI technique implemented to isolated 1D structures seems to be robust and stable, even in cases where the LIN code meets certain difficulties with the convergence. For practical use, the efficiency can be further improved using a suitable acceleration scheme (Ng, ORTHOMIN).

Similarly as in LIN/PRD code of HGV, we plan to combine the present MALI code with ETLA-based PRD iterations in order to account for PRD in resonance Lyman lines and for Raman scattering. In this way we can investigate an importance of PRD-interlocking effects, as was recently done by Hubeny & Lites (1994) for the quiet solar chromosphere. Generalization of the present approach to other geometries (2D slabs) is rather straightforward and requires an efficient method for formal solution of the transfer equation (Paletou 1994). Because of its speed efficiency, MALI can be also used in a combination with the IBC method of Heinzel (1991) to treat inhomogeneous atmospheres.

In subsequent papers we shall apply our MALI approach to various isolated structures and perform NLTE computations for chemical species other than hydrogen.

Acknowledgements. A substantial part of this work has been done during author's stay at Observatoire de Meudon. He would like to express

his gratitude for useful discussions, support and kind hospitality. Most computations have been performed on Digital VAX Station 3100 at DASOP-URA326. The author is indebted to Dr. I. Hubeny for critical reading of the manuscript. Several discussions with colleagues from IAS (Orsay) and HAO (Boulder), particularly with Dr. F. Paletou, are also highly acknowledged.

This article was processed by the author using Springer-Verlag L^AT_EX A&A style file version 3.

References

- Auer L.H., 1967, *ApJ* 150, L53
 Auer L.H., 1991, in: Crivellari L., Hubeny I., Hummer D.G. (eds.) *Stellar Atmospheres: Beyond Classical Models*, NATO-ASI Series C 341, Kluwer Acad. Publ., Dordrecht, 9
 Auer L.H., Mihalas D., 1969, *ApJ* 158, 641
 Auer L.H., Paletou F., 1994, *A&A* 285, 675
 Avrett E.H., Loeser R., 1987, in: Kalkofen W. (ed.) *Numerical Radiative Transfer*, Cambridge Univ. Press, Cambridge, 135
 Crivellari L., Hubeny I., Hummer D.G. (eds.), 1991, *Stellar Atmospheres: Beyond Classical Models*, NATO-ASI Series C 341, Kluwer Acad. Publ., Dordrecht
 Fontenla J.M., Reichmann E.J., Tandberg-Hanssen E., 1988, *ApJ* 329, 464
 Gouttebroze P., Heinzel P., Vial J.-C., 1993, *A&AS* 99, 513 (GHV)
 Heinzel P., 1983, *Bull. Astron. Inst. Czechosl.* 34, 1
 Heinzel P., 1991, in: Crivellari L., Hubeny I., Hummer D.G. (eds.) *Stellar Atmospheres: Beyond Classical Models*, NATO-ASI Series C 341, Kluwer Acad. Publ., Dordrecht, 297
 Heinzel P., Schmieder B., 1994, *A&A* 282, 939
 Heinzel P., Gouttebroze P., Vial J.-C., 1987, *A&A* 183, 351 (HGV)
 Heinzel P., Gouttebroze P., Vial J.-C., 1994, *A&A* 292, 656
 Heinzel P., Schmieder B., Mein P., 1992, *Solar Phys.* 139, 81
 Hubeny I., 1985, *Bull. Astron. Inst. Czechosl.* 36, 1
 Hubeny I., 1992, in: Heber U., Jeffery C.J. (eds.) *The Atmospheres of Early-Type Stars*, *Lecture Notes in Phys.* 401, Springer-Verlag, Berlin, 377
 Hubeny I., 1994, private communication
 Hubeny I., Lites B., 1994, *ApJ* in press
 Kalkofen W. (ed.), 1987, *Numerical Radiative Transfer*, Cambridge Univ. Press, Cambridge
 Mihalas D., 1978, *Stellar Atmospheres*, 2nd edn., W.H. Freeman, San Francisco
 Mihalas D., Heasley J.N., Auer L.H., 1975, *A Non-LTE Model Stellar Atmosphere Computer Program*, NCAR-TN/STR-104, HAO-NCAR, Boulder
 Olson G.L., Auer L.H., Buchler J.R., 1986, *JQSRT* 35, 431 (OAB)
 Paletou F., 1994, *A&A* submitted
 Paletou F., Vial J.-C., Auer L.H., 1993, *A&A* 274, 571
 Rovira M.G., Fontenla, J.M., Vial J.-C., Gouttebroze P., 1994, in: Rušin V., Heinzel P., Vial J.-C. (eds.) *Solar Coronal Structures*, *Proc. IAU Coll.* 144, Veda Publ. House, 315
 Rušin V., Heinzel P., Vial J.-C. (eds.), 1994, *Solar Coronal Structures*, *Proc. IAU Coll.* 144, Veda Publ. House, Slovak Acad. Sci.
 Ruždjak V., Tandberg-Hanssen E. (eds.), 1990, *Dynamics of Quiescent Prominences*, *Proc. IAU Coll.* 117, *Lecture Notes in Phys.* 363, Springer-Verlag, Berlin
 Rybicki G.B., Hummer D.G., 1991, *A&A* 245, 171 (RH1)
 Rybicki G.B., Hummer D.G., 1992, *A&A* 262, 209 (RH2)
 Schmieder B., Heinzel P., Wiik J.E., Lemen L., Anwar B., Kotrč P., Hiei E., 1994, *Solar Phys.* in press
 Wiik J.E., Heinzel P., Schmieder B., 1992, *A&A* 260, 419